Photoelectron-Photofragment Angular Correlation and Energy Partitioning in Dissociative Photodetachment

K. A. Hanold, M. C. Garner, and R. E. Continetti
Department of Chemistry and Biochemistry, 0314, University of California, San Diego, 9500 Gilman Drive, La Jolla, California 92093-0314
(Received 10 June 1996)

Measurements of photoelectron-photofragment angular correlation and energy partitioning in the dissociative photodetachment of O_4^- ($O_4^- + h\nu \rightarrow O_2 + O_2 + e^-$) at 532 nm are reported. Using photofragment translational energy and photoelectron spectroscopy in coincidence, vibrationally resolved product translational energy distributions and a pronounced angular correlation between the photoelectron and photofragment recoil directions are observed. These results provide insights into the molecule-fixed photoelectron angular distribution of a negative ion and structural information on O_4^- in the gas phase. [S0031-9007(96)01411-1]

PACS numbers: 33.80.Eh

The dynamics of photodetachment and photoionization processes are sensitive probes of electron-molecule interactions. Photoelectron angular distributions provide detailed information on photodetachment dynamics due to the fact that they are a function of both the magnitude and relative phases of the degenerate electron continuum channels accessible in photodetachment processes [1,2]. Studying the photoelectron angular distribution in the *molecular* frame provides greater insights into the photodetachment dynamics. This results from the removal of the averaging over molecular orientations inherent in a laboratory angular distribution. Theoretical studies of such molecule-fixed photoelectron angular distributions (MF-PAD) have been pursued for an improved understanding of the dynamics of photoionization [1,3–6] and electron interactions with molecules oriented on surfaces [7]. Evidence of anisotropic MF-PAD's have been observed in experiments on the dissociative photoionization of H_2 [8], O_2 [9], and several halomethanes [10,11]. Direct detailed measurements of the MF-PAD in the photoionization of NO have recently been reported [5]. Measurements of the MF-PAD for the photodetachment of negative ions are of interest as they will provide insights into the nature of both the bound electron in the anion and the anisotropy of electron-molecule interaction potentials.

The structure and energetics of atomic and molecular cluster anions have received considerable attention in recent years. Translational energy spectroscopy can be used to determine bond energies and photofragment internal energy distributions [12]. Photoelectron kinetic energy spectroscopy has been used to characterize vibrational and electronic states of both anionic and neutral clusters [13]. In many systems, however, photodetachment produces the neutral far from the equilibrium geometry. The repulsive energy in the cluster can then lead to rapid dissociation. To study the dissociation dynamics of such short-lived neutral clusters, it is essential to measure the photoelectron kinetic energy *and* the translational energy released between the atomic or molecular fragments. Such measurements can reveal both the internal energy distribution of the photofragments and provide a direct measure of the repulsive energy in the complex. In this Letter, we report measurements in which a complete kinematic description of dissociative photodetachment (DPD) is obtained by the simultaneous measurement of the kinetic energy and recoil angle of the photoelectron and photofragments in the reaction $O_4^- + h\nu \rightarrow O_2 + O_2 + e^-$ at 532 nm (2.33 eV). The data reveal both vibrationally resolved translational energy distributions and evidence of an anisotropic MF-PAD in negative ion photodetachment for the first time.

O_4^- has been studied previously using photoelectron spectroscopy [14] and translational energy spectroscopy [15,16]. The photoelectron kinetic energy spectrum at 532 nm shows a broad, structureless peak centered at 0.7 eV with a full width at half maximum (FWHM) of 0.3 eV. The structureless spectrum is in marked contrast to the vibrationally resolved photoelectron spectrum of O_2^- at this wavelength. This shows that the structure of O_4^- is not well characterized as a weakly interacting $O_2 \cdots O_2^-$ complex. The photoelectron angular distribution is peaked perpendicular to the electric vector **E** of the laser beam [14]. The photofragment translational energy release spectrum is dominated by a large peak centered at 0.4 eV. This feature has been shown to result from the DPD of O_4^-. The photofragment angular distribution for this dissociative photodetachment process is also peaked perpendicular to the **E** vector [15].

In the present experiments, photoelectron spectroscopy is used in coincidence with photofragment translational energy spectroscopy in a fast negative-ion beam to measure the partitioning of translational energy between the three particles produced in DPD of O_4^-. A schematic of the detection geometry is shown in Fig. 1. The simultaneous determination of recoil angles and kinetic energies for all three particles is achieved with this apparatus. The photoelectron [17] and photofragment translational [15] spectrometers have been described in detail previously and will only be briefly described here. Anions are produced

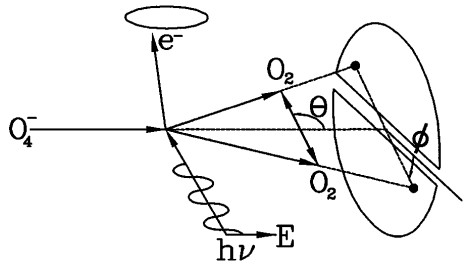

FIG. 1. Schematic of the experimental geometry for detection of $O_2 + O_2 + e^-$. Photofragment center-of-mass scattering angles θ and ϕ are indicated in the figure.

and cooled in a pulsed free jet expansion of O_2 intersected by a 1 keV electron beam. The anions are accelerated to an energy of 3 keV and mass selected by time of flight. Anions at the mass of interest are intersected by a pulsed 200 μJ/pulse, 100 ps FWHM, linearly polarized 532 nm laser beam [18].

Photoelectrons traverse a field-free flight path of 75 mm and impinge on an 80 mm diameter detector centered perpendicular to the **E** vector. The laboratory kinetic energy is measured by time of flight and the electron recoil angle by position. The photoelectron spectrometer has an effective angular acceptance of $\approx$4% of 4π sr. The center-of-mass electron kinetic energy (eKE) resolution is $\approx$4% $\Delta E/E$ and the electron angular resolution is $\approx$35 mrad.

Photofragments recoil out of the beam over a 96 cm flight path between the laser interaction and the photofragment detector. The photofragments that clear a 7-mm-wide beam block impinge on the 40 mm diameter detector. The time and position of arrival of the two photofragments determine the fragment mass ratio, center-of-mass translational energy (E_T), and recoil angle of each fragment. The translational energy resolution is $\leq$10% $\Delta E/E$ at $E_T = 0.55$ eV. Photofragment recoil angular resolution is estimated to be $\approx$10 mrad. The angular acceptance of this detector is two opposing semicircles, each covering $\approx$40% of 4π sr given the kinematics of O_4^- dissociation into $O_2 + O_2 + e^-$.

Each event is required to consist of two neutral fragments *or* two neutral fragments and an electron. Residual ions and ionic photofragments were electrostatically deflected out of the beam. Checking for conservation of linear momentum between the two photofragments ensures that they originate in a single dissociative event. Correlation of the photoelectron and the neutral photofragments is determined by the spectrometer efficiency and the count rate. With the spectrometer operating at 600 Hz, and the observed triple coincidence rate of 0.25 Hz, false photoelectron-neutral-neutral coincidences contribute $\approx$ 4% of the triple coincidence data presented here.

The (eKE, E_T) correlation spectrum is shown in Fig. 2. This contour map reveals a series of at least four diagonal ridges, centered at $E_T = 0.4$ eV, and a vertical row of spots at $E_T = 0.8$ eV. The eKE values of the spots in the vertical row at $E_T = 0.8$ eV are consistent with the known eKE peaks in the O_2^- photoelectron spectrum [19]. These features arise from a second photon detaching the electron from an $O_2^-(X^2\Pi_g)$ photofragment produced in the photodissociation of O_4^- [$O_4^- + h\nu \rightarrow O_2(^1\Delta_g) + O_2^-(X^2\Pi_g)$].

The more interesting features in this correlation spectrum are the diagonal ridges. Energy conservation dictates that all events that lie within a single diagonal ridge have a well-defined total kinetic energy ($E_{\text{tot}} = E_T + \text{eKE}$). Within a given ridge, however, there is a range of kinetic energy partitioning between the three products. Using the dissociation energy of O_4^- into $O_2 + O_2^-$ (0.46 eV [20]) and the electron affinity O_2 (0.45 eV [19]), one can calculate the maximum translational energy for the DPD to be 1.42 eV. This is marked as limit (*A*) in Fig. 2.

The product O_2 vibrational distribution can be examined by measuring E_{tot}. As the E_{tot} spectrum in Fig. 3 shows, the diagonal ridges in the correlation spectrum of Fig. 2 appear as well-resolved peaks. The limit (*A*) is shown as a vertical line in Fig. 3 and corresponds to the origin of the internal energy axis shown at the top of the figure. The spacing of the first five vibrational levels of O_2 are shown as combs on the spectrum for reference. The offset of the vibrational peaks from the internal energy origin gives an average rotational energy of the photofragments of 80 $\pm$ 30 meV. The width of these peaks indicates a narrow range of rotational excitation for the two O_2 products, implying that O_4^- dissociates from a well-defined structure.

Spectroscopic studies of matrix-isolated O_4^- have indicated that the structure is a centrosymmetric *trans*-planar species of C_{2h} symmetry with a delocalized negative

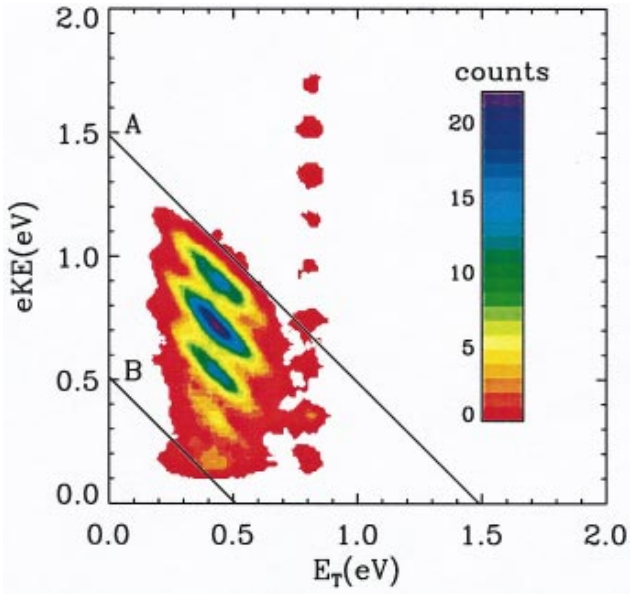

FIG. 2(color). (eKE, E_T) correlation spectrum for O_4^- at 532 nm (2.33 eV). Contours are linearly scaled, with counts representing the number of coincident events in each 10 $\times$ 10 meV bin. Energetic limits are shown for (*A*) $O_2(X^3\Sigma_g^-) + O_2(X^3\Sigma_g^-) + e^-$ and (*B*) $O_2(X^3\Sigma_g^-) + O_2(a^1\Delta_g) + e^-$.

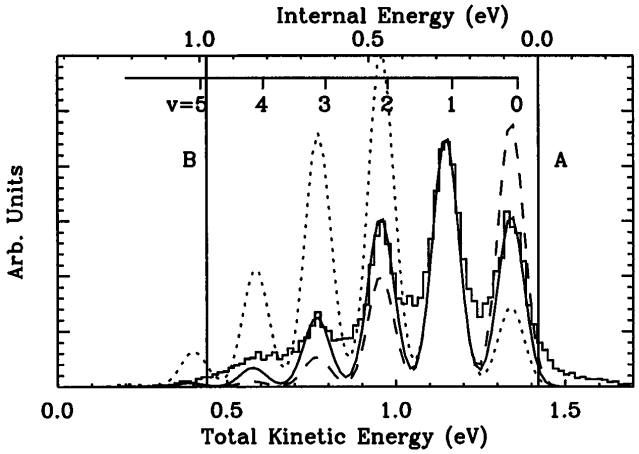

FIG. 3. Total kinetic energy spectrum for dissociative photodetachment events. Energetic limits are the same as those shown in Fig. 1. The top axis indicates the internal energy. The data is represented by points, the solid-line fit to the data assumes two equal bond length O_2 moieties of 1.272 Å. The dashed-line fit assumes unequal O_2 moiety bond lengths of 1.23 and 1.33 Å, while the dotted-line fit assumes equal bond lengths of 1.26 Å. The fits are normalized to the $v = 1$ peak.

charge [21]. The observation of vibrational structure in the E_{tot} spectrum allows structural inferences on gas-phase O_4^- to be made. A simple simulation was performed by calculating the Franck-Condon overlap of the vibrational wave functions of two perturbed O_2 molecules with two free $O_2(X^3\Sigma_g^-)$ (equilibrium bond length 1.207 Å [22]). The agreement between the simulation, assuming equal bond lengths of 1.272 Å, and the data is excellent as shown in Fig. 3. The sensitivity of the simulation to changes in the bond lengths of the perturbed O_2 is shown by the textured curves in Fig. 3. These results are qualitatively consistent with the matrix studies and preliminary density functional calculations of the O_4^- structure [23].

The angular distributions of the $O_2 + O_2 + e^-$ photoproducts are observed to be highly anisotropic. Photodetachment or photodissociation of an isotropic ensemble of molecules is known to yield photoelectron or photofragment angular distributions given by the equation [2,24]

$$I(\theta) = \frac{d\sigma}{d\Omega} = \frac{\sigma}{4\pi}[1 + \beta P_2(\cos\theta)]. \qquad (1)$$

In this equation, σ is the total cross section and $P_2(\cos\theta)$ is a Legendre polynomial, where θ is the polar angle between the photofragment recoil and the electric vector of the laser. The anisotropy parameter β is restricted to have values between -1 [$I(\theta) \propto \sin^2\theta$] and $+2$ [$I(\theta) \propto \cos^2\theta$]. Both photoelectrons and O_2 photofragments produced in the DPD of O_4^- are preferentially scattered in the plane perpendicular to the **E** vector ($\beta \approx -0.8$ and -0.9 for photofragments and photoelectrons, respectively) [14,15].

In these experiments, the recoil angles for the photoelectron and photofragments are measured *in coincidence*, yielding the angular correlation between these three particles and the **E** vector. A pronounced angular correlation is observed which may be understood by considering Fig. 1. As this schematic diagram shows, the **E** vector lies along the ion beam. Detection of an electron in coincidence requires that the electron recoil into a cone above the plane of the laser and ion beam, breaking the cylindrical symmetry about the **E** vector and the ion beam. The E_T-integrated DPD photofragment angular distribution, $N_n(\theta, \phi)$, is extracted by integrating the data over $0 < E_T < 0.6$ eV to give the number of events as a function of θ and ϕ. In this notation, n denotes the number of particles detected in coincidence; $n = 2$ for $O_2 + O_2$ and $n = 3$ for $O_2 + O_2 + e^-$ and ϕ is the azimuthal angle around the **E** vector. Frame A of Fig. 4 shows a surface-density plot of $N_2(\theta, \phi)$ in the coordinate frame shown in frame D. Given that the O_2 photofragment angular distribution is nearly $\sin^2\theta$, with $\beta = -0.8$, this resembles a torus with a strip cut out of the middle due to the acceptance of the photofragment detector. Electrons are only detected when they recoil in a small cone perpendicular to the plane defined by the laser and ion beams in the laboratory. If there is an angular correlation between the photofragments and the photoelectrons, $N_3(\theta, \phi)$ for the O_2 photofragment pairs in the $O_2 + O_2 + e^-$ coincidence data will differ from $N_2(\theta, \phi)$. $N_3(\theta, \phi)$ is shown in frame B of Fig. 4. A pronounced reduction of $O_2 + O_2$ photofragment recoils detected parallel to the direction of electron recoil is observed. This angular correlation shows that photodetachment and dissociation of the nuclear framework of O_4 both occur on time scales fast relative to molecular rotation ($\approx$1–10 ps). Thus, by measuring the asymptotic recoil direction of the O_2 photofragments, the spatial direction of the dissociating bond at the time of photon absorption is determined. These results show that the photoelectron preferentially recoils *perpendicular* to the breaking bond in O_4.

This angular correlation is an obvious manifestation of an anisotropic MF-PAD. As first discussed by Dill [3] in reference to the photoionization of diatomic molecules, the MF-PAD contains considerably more information than the laboratory angular distributions. In contrast to Eq. (1), the MF-PAD in general depends on both polar and azimuthal angles. The strong angular correlation observed between photoelectron and photofragments indicates that the photoelectron continuum is dominated by a restricted set of partial waves. Direct extraction of the MF-PAD from this data requires modeling the photoelectron detector angular acceptance, and will be described in a forthcoming paper.

The nature of the photoelectron-photofragment angular correlation can be further visualized by considering the photofragment angular distribution in the electron-recoil frame, as opposed to the **E** vector frame. This distribution can be easily generated by dividing $N_3(\theta, \phi)$ by $N_2(\theta, \phi)$. This has the effect of removing from $N_3(\theta, \phi)$ weighting due to both the photofragment angular distribution in $N_2(\theta, \phi)$ and the finite angular acceptance of the

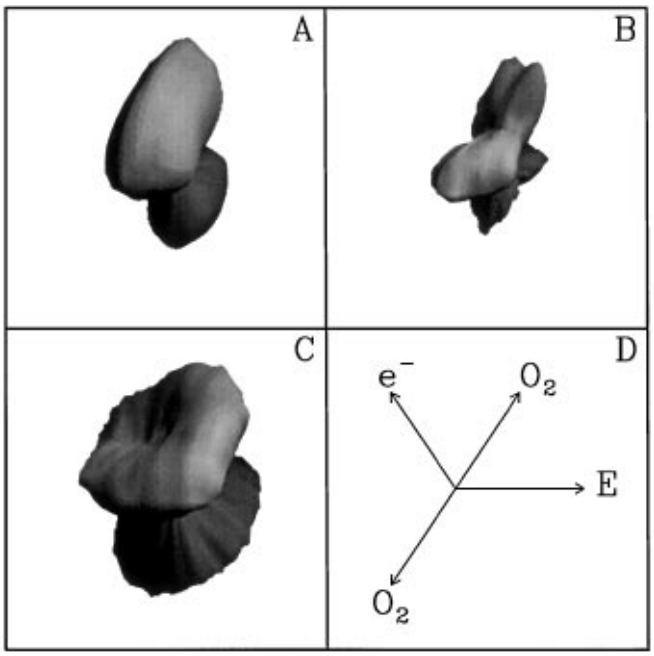

FIG. 4. Surface-density plots of the energy-integrated angular distributions of O_2 photofragments. The number of events is shown as the distance of the surface from the origin. Frame A shows the experimentally observed photofragment distribution $N_2(\theta, \phi)$ for detection of coincident O_2 photofragments. Frame B shows the experimentally observed photofragment distribution $N_3(\theta, \phi)$ for the coincident detection of two photofragments and an electron. Frame C shows the photofragment distribution relative to the electron ejection direction $N_3(\theta, \phi)/N_2(\theta, \phi)$. Frame D shows the nominal direction of the **E** vector, the photoelectron and photofragment recoil directions.

photofragment detector. This treatment presumes that the photoelectron recoils at a single nominal angle in the laboratory frame. As the distribution in frame C of Fig. 4 shows, the electron-recoil-frame photofragment angular distribution also resembles $\sin^2\theta'$, where θ' is defined as the polar angle of photofragment recoil relative to the nominal electron-recoil direction. The presence of the photofragment detector beam block prevents detection of the most intense part of this angular distribution at $\theta' = 90°$. A fit by Eq. (1) shows that this distribution is characterized by $\beta \approx -0.5$. Because of the assumption of a nominal electron-recoil laboratory angle, this is an upper bound on this anisotropy parameter.

This Letter reports the first high-resolution energy and angle-resolved experiments on the dissociative photodetachment of a cluster anion. Because of the rapid dissociation of O_4^- after photon absorption, measurement of the photoelectron and photofragment translational energies in coincidence is required to reveal the energy partitioning to vibrational degrees of freedom of the O_2 products. A simple Franck-Condon model shows that the product vibrational distribution is sensitive to the structure of O_4^-. Detailed information on the electronic structure of this open-shell negative ion is required to apply the existing formalisms for the MF-PAD. The observation that the MF-PAD peaks perpendicular to the dissociating bond will provide an important test of such calculations. In the case of photodetachment, the dynamics of electron departure will also be influenced by effects such as electron correlation. Further work on the measurement and interpretations of the MF-PAD in this and other negative ions can thus be expected to provide new perspectives on electron-molecule interactions.

This work was supported by the National Science Foundation, the David and Lucile Packard Foundation (Fellowship in Science and Engineering), and the Camille and Henry Dreyfus Foundation (New Faculty Award). Professor John Simon is acknowledged for providing the laser used in this study.

[1] N. Chandra, Chem. Phys. **108**, 301 (1986).
[2] J. Cooper and R. N. Zare, J. Chem. Phys. **48**, 942 (1968).
[3] D. Dill, J. Chem. Phys. **65**, 1130 (1976).
[4] H. Rudolph and V. McKoy, J. Chem. Phys. **91**, 2235 (1989).
[5] H. K. Park and R. N. Zare, J. Chem. Phys. **104**, 4554 (1996), and references therein.
[6] K. L. Reid and I. Powis, J. Chem. Phys. **100**, 1066 (1994).
[7] R. E. Palmer and P. J. Rous, Rev. Mod. Phys. **64**, 383 (1992).
[8] J. L. Dehmer and D. Dill, Phys. Rev. A **18**, 164 (1978).
[9] A. V. Golovin, N. A. Cherepkov, and V. V. Kuznetsov, Z. Phys. D **24**, 371 (1992).
[10] I. Powis, Chem. Phys. Lett. **189**, 473 (1992).
[11] S. Kaesdorf, G. Schönhense, and U. Heinzmann, Phys. Rev. Lett. **54**, 885 (1985).
[12] J. M. Farrar, in *Cluster Ions,* edited by T. Baer, C. Y. Ng, and I. Powis (Wiley, New York, 1993), pp. 243–317.
[13] S. T. Arnold *et al.*, in *Ion and Cluster Ion Spectroscopy and Structure,* edited by J. P. Maier (Elsevier, New York, 1989), pp. 417–472.
[14] M. J. DeLuca, C. C. Han, and M. A. Johnson, J. Chem. Phys. **93**, 268 (1990); C.-C. Han and M. A. Johnson, Chem. Phys. Lett. **189**, 460 (1992).
[15] C. R. Sherwood *et al.*, J. Phys. Chem. **102**, 6949 (1995).
[16] K. A. Hanold, C. R. Sherwood, and R. E. Continetti, J. Chem. Phys. **103**, 9876 (1995).
[17] K. A. Hanold, C. R. Sherwood, M. C. Garner, and R. E. Continetti, Rev. Sci. Instrum. **66**, 5507 (1995).
[18] X. Xie and J. D. Simon, Opt. Commun. **69**, 303 (1989).
[19] M. J. Travers, D. C. Cowles, and G. B. Ellison, Chem. Phys. Lett. **164**, 449 (1989).
[20] K. Hiraoka, J. Chem. Phys. **89**, 3190 (1988).
[21] L. Manceron, A-M. Le Quere, and J.-P. Perchard, J. Phys. Chem. **93**, 2960 (1989).
[22] K. P. Huber and G. Herzberg, *Molecular Spectra and Molecular Structure IV* (Van Nostrand, New York, 1979) p. 490.
[23] K. Morokuma (private communication).
[24] R. N. Zare, Mol. Photochem. **4**, 1 (1972).